Thin-Shell Deployable Reflectors with Collapsible Stiffeners:
Part I – Approach

Lin Tze Tan[*]

University College London, London WC1E 6BT, England, United Kingdom

Sergio Pellegrino[†]

University of Cambridge, Cambridge CB2 1PZ, England, United Kingdom

Thin-shell deployable reflector structures that are folded elastically in a nearly-inextensional mode have been recently realized, exploiting the recent availability of high-modulus, ultra-thin composite materials. An inherent, and significant limitation of this approach is that these structures remain "floppy" in their deployed configuration. This paper presents a general concept for increasing the deployed stiffness of such structures, through the addition of a collapsible edge stiffener around the rim of a reflector dish. An analytical expression of the frequency/stiffness related to the softest deformation mode of a thin-shell reflector structure is presented, both with and without the stiffener. During folding, the stiffener collapses elastically, and this behaviour is facilitated by the introduction of suitable discontinuities within the stiffener, or between the dish and the stiffener. A detailed study of a range of different options is presented, and one particular scheme is selected and optimized. For a specific example, a stiffness increase by a factor of 31 and a fundamental frequency increase by a factor of 4 are achieved, with a mass increase of only 16%.

[*]Lecturer in Structural and Solid Mechanics, Department of Civil Engineering, Gower Street, `l.tan@ucl.ac.uk`, Member of AIAA

[†]Professor of Structural Engineering, Department of Engineering, Trumpington Street, `pellegrino@eng.cam.ac.uk`, Associate Fellow of AIAA

Nomenclature

A_i	amplitude of mode i
B	breadth of rim
b	breadth of rectangular cross-section
c	radius of coiling
D	plate bending stiffness pg. 9 and 10, aperture diameter (pg. 13 onwards)
d	diameter of tubular cross-section
E	Young's modulus
F_{final}, F_{max}	final packaged force, maximum force
f_i	frequency of mode $(i-1)$
F	focal length of paraboloid
f	fundamental frequency
g_1, g_2	dimensionless parameters for calculation of natural frequencies of spherical shells
h	height of rectangular cross-section
h_0	height of rim
I_R, I_T	second moment of areas of rectangular section and tubular section
k	initial stiffness
r, r_s	radius, radius of mid surface of spherical shell
T	depth of rim
t	thickness of shell
U	strain energy
V	kinetic energy
w	width of stiffener

Symbols

η	slit angle
γ	slit angle
ν	Poisson's ratio
ϕ, ϕ_0, ϕ_1	angles that define general parallel of shell, rim of shell, and inner edge of stiffener
ρ	density
$\sigma, \sigma_{max}, \sigma_y$	stress, maximum stress in packaged configuration, yield stress
θ	angle that defines a meridian of the shell

I.   Introduction

Thin-walled deployable structures have been used for a variety of spacecraft structures and, until recently, almost only in the form of singly-curved shell structures. Notable ex-

amples include tubular metallic booms such as the Storable Tubular Extendible Mast[1] and the Collapsible Tube Mast,[2] and self-locking hinges consisting of short lengths of steel tape measure (tape springs) for solar arrays.[3] A feature that is common to all of these foldable structures is that they undergo a continuous process of inextensional elastic deformation that transforms the structure from its operational configuration into a compactly packaged configuration.

The recent availability of high-modulus, ultra-thin composite materials has led to the realization of structures with greater functionality, through the use of complex three-dimensional shapes. Novel applications of this approach to deployable reflector structures have been proposed.[4–6]

An example of particular relevance to the present paper is the Spring Back Reflector,[7,8] an ultra thin flexible parabolic shell made from triaxially woven carbon-fibre reinforced plastic (CFRP). The whole structure, shown in Figure 1, is manufactured as a single piece, and hence without any expensive and potentially unreliable joints; it has a diameter of about 6 m, thickness varying between 0.3 mm and 3.2 mm, and a total mass of around 20 kg.

The folding concept[9] is both simple and effective: opposite edges of the reflector are pulled towards each other by about half of their original distance, and thus the reflector becomes folded elastically, as shown in Figure 1. Once in orbit, the tie cables that hold the reflector in its packaged configuration are cut, and the reflector deploys by releasing its stored strain energy.

Figure 1. MSAT-2 spacecraft during ground testing with two Spring-Back Reflectors, one deployed and one folded. Courtesy of Canadian Space Agency.

Intuitively, a "floppy" structure is more likely to survive this process undamaged than a "stiff" structure, but reflector structures of low stiffness have poor shape accuracy[10] and are also prone to becoming dynamically coupled with the attitude control of the spacecraft. Both of these limitations would severely restrict the potential range of applications.

This paper proposes a modification of the Spring Back Reflector concept, based on the idea of adding a thin-walled stiffening element around the edge of the dish. This element significantly increases the overall stiffness of the dish in the deployed configuration, and yet it is engineered in such a way that the stiffened dish can still be folded elastically. A detailed description of the stiffening concept together with the subtleties that are required to make this approach work are presented.

The paper is presented in seven sections plus an appendix. Following the present introduction, Sections II and III explain the concept of exploiting geometrically non-linear effects through which an elastic structure becomes softer while it is folded. The concept is illustrated by comparing two different designs for a coilable cantilever beam. It is shown that a beam whose cross-section can be flattened prior to coiling can be several orders of magnitude stiffer than a standard, rigid cross-section beam of equal mass. Section IV presents a straightforward extension of Rayleigh's classical work on the vibration of thin spherical shells, leading to an approximate, analytical expression for the natural frequencies of vibration of a spherical cap with an edge stiffener. The fundamental natural frequency ratio —which is a measure of the stiffness increase achieved divided by the mass penalty— can thus be estimated. The range of applicability of this result is discussed and its accuracy is assessed. With this background, Section V carries out a detailed study of 7 different configurations of the edge stiffener, for the particular case of a small scale dish. For each configuration, detailed finite-element simulations of the folding process are performed in order to estimate the deployed fundamental natural frequency, initial stiffness of the reflector, packaging force characteristics and the maximum stresses in the packaged configuration. For some selected configurations, the sensitivity of these results to two key design parameters of the stiffener is determined. This work leads to the choice of a specific configuration of the stiffener, consisting of a conical-section ring that is attached to the rim of the reflector, but left disconnected at four locations. In practice, the edge stiffener would be made as an integral part of the structure, and four slits would be cut along the connection between the two surfaces. Section VI presents an optimized version of the configuration selected in the previous section. Section VII concludes the paper. The Appendix presents a derivation of the spherical equivalent to a dish of parabolic shape.

Tan & Pellegrino

II. Structures that Become Softer during Folding

Consider a general deployable structure made of linear-elastic material, which is assumed to deform according to a linear force-displacement relationship when it is folded. Here, the displacement variable is a parameter that describes the configuration of the structure, and the force variable is the corresponding value of the external action(s) required to keep the structure in static equilibrium in each particular configuration. Now, consider a modified design of this structure which is (i) stiffer than the initial design and (ii) follows the same deformation mode when it is folded as the initial design. The force-displacement relationships of the two designs are schematically shown by the two dashed straight lines labelled 'softer' and 'stiffer' in Figure 2.
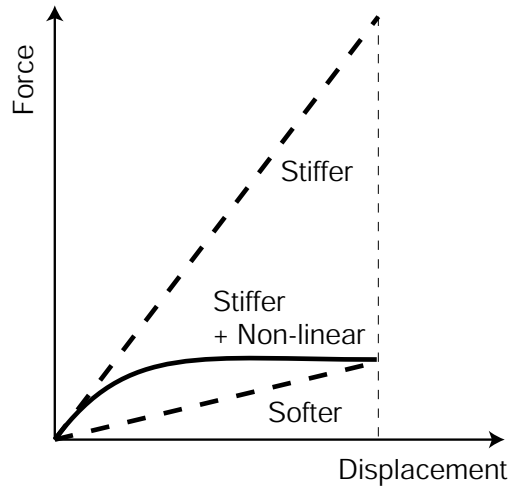
Figure 2. **Schematic of folding force-displacement relationships for linear and non-linear structures.**

Since the "stiffness" of the structure has been increased, the slope of the force-displacement relationship will be higher. Furthermore, since the final value of the displacement parameter in the folded configuration is the same, the total amount of strain energy required to fold the structure will increase proportionally with its stiffness.

Now, if it is further assumed that the folding of the structure can be modelled as a process that involves purely beam-bending deformation, two extreme ways of achieving the stiffness increase are (i) to increase the width of the bending elements, in which case the stiffness increase is directly proportional to the width increase, or (ii) to increase their thickness, in which case the stiffness increases with the cube of the thickness. In terms of mass efficiency, case (ii) is clearly superior to (i) but the maximum bending stress in the folded configuration will also increase in proportion to the thickness. In fact, neither scheme is ideal for lightweight deployable structures.

In deployable structures of simple shape it is already well known that the best way of

Tan & Pellegrino

designing for high deployed stiffness and low maximum stress in the folded configuration is to exploit geometrically non-linear behaviour. This can be achieved, for example, by allowing a thin-walled, transversally curved strip to become flatter as it begins to fold. Further details are given in the next section.

III.   Coilable Beams

In this section we consider the simple problem —simple in the sense that it admits a full analytical solution— of designing a straight, uniform metallic beam that can be coiled uniformly, without yielding. For a given radius of coiling, c, we compare the stiffest possible design that can be achieved for a beam with rectangular cross-section with an alternative design based on a slit circular tube, as in Figure 3. This alternative design allows the beam cross-section to be flattened before being coiled. Both the total cross-sectional area and the material of the beam, and hence the mass of both designs, are the same.

In the rectangular cross-section beam of breadth, b and height, h, the maximum stress in the coiled configuration is

$$\sigma = \frac{Eh}{2c} \tag{1}$$

where E is the Young's modulus. If the maximum allowable value for σ is the yield stress σ_y, then the maximum value of h is

$$\overline{h} = 2c\sigma_y/E \tag{2}$$

and the bending stiffness of this maximally stiff rectangular-section beam is —neglecting the modulus—

$$I_R = b\overline{h}^3/12 = \frac{2}{3}bc^3 \left(\frac{\sigma_y}{E}\right)^3 \tag{3}$$

Next, consider a tubular beam whose cross-section has diameter, d, thickness, t, and is split at the top. To make its cross-sectional area, and hence its mass, equal to that of the previous beam we set

$$b\overline{h} = \pi dt \tag{4}$$

and so, solving for d and substituting Equation 2,

$$d = 2bc\sigma_y/\pi Et \tag{5}$$

The value of t can be determined by requiring that this beam be on the point of yielding (according to the Tresca yield condition) when its cross-section is flattened and the beam is

Tan & Pellegrino
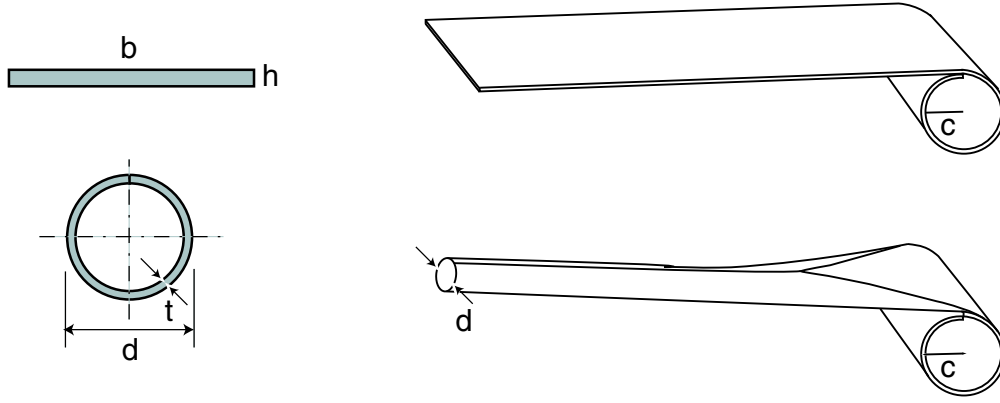
Figure 3. Coilable beams with rectangular and tubular cross-sections.

longitudinally coiled. Rimrott[1] has shown that this condition requires

$$\frac{d}{t} = \frac{E}{\sigma_y} \frac{(2c/d) + \nu}{(1 - \nu^2)(2c/d)} \tag{6}$$

where ν is the Poisson's ratio.

Substituting Equation 5 into Equation 6, one obtains a quadratic equation in t, which has the solution

$$t = \left(\sqrt{\left(\frac{\nu}{2\pi}\right)^2 + \frac{2(1 - \nu^2)}{\pi} \frac{c}{b}} - \frac{\nu}{2\pi} \right) \frac{\sigma_y}{E} b \tag{7}$$

When this beam is uncoiled, its bending stiffness —again neglecting the Young's modulus— is

$$I_T \approx \frac{\pi d^3 t}{8} \tag{8}$$

where d and t can be obtained from Equations 5 and 7.

To compare the static stiffness of these two beams, consider the ratio I_T/I_R, which can be shown to have the expression

$$\frac{I_T}{I_R} = \frac{3}{2\pi^2} \left(\frac{E}{\sigma_y}\right)^2 \Bigg/ \left(\sqrt{\left(\frac{\nu}{2\pi}\right)^2 + \frac{2(1 - \nu^2)}{\pi} \frac{c}{b}} - \frac{\nu}{2\pi} \right)^2 \tag{9}$$

For equal mass beams the ratio I_T/I_R is inversely proportional to the the radius of coiling, c, divided by the breadth of the original rectangular section, b, and is directly proportional to the squared ratio of the modulus divided by the yield stress. Note that this latter proportion (E/σ_y) has typical values of 50-200 for most structural materials.

Equation 9 has been plotted for $E/\sigma_y = 100$ in Figure 4. The plot shows that the stiffness ratio is in excess of 200, even for loosely coiled beams, and much larger for more tightly coiled beams.

Tan & Pellegrino
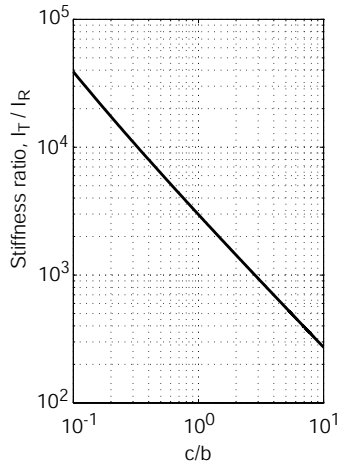
Figure 4. Variation of flexural stiffness of maximally stiff tubular beam with respect to stiffness of rectangular cross-section beam, for $E/\sigma_y = 100$.

This example has shown that a beam with a rectangular cross-section is much less stiff than a beam of equal mass whose tubular cross-section can be flattened prior to coiling. Non-circular cross-sections could provide even stiffer designs, but the example presented above has demonstrated the potential advantages of designing thin-walled foldable structures with stiffening elements that increase the stiffness of the deployed structure, but can be elastically collapsed prior to folding.
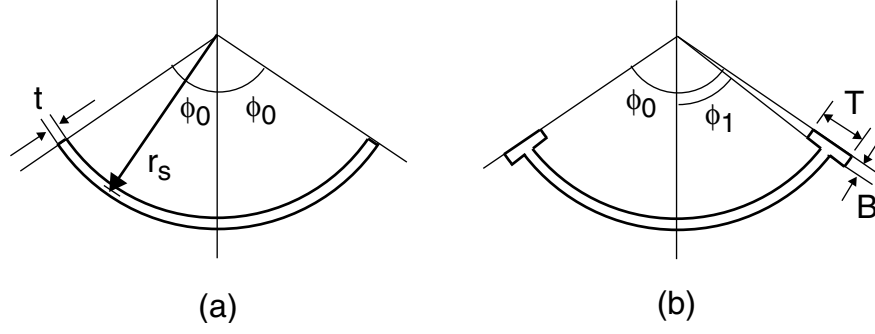
IV. Spherical Caps

The stiffness of a parabolic dish can be increased in many different ways. An obvious way is increasing the thickness of the dish uniformly; other options are adding a solid ring beam around the rim of the dish, or adding a series of radial/hoop ribs, etc. We are interested in choosing a solution that requires only a very small increase in mass to provide a large increase in stiffness, and the most effective way of doing this is adding a thin-walled stiffener around the rim.

We show this by investigating how the fundamental natural frequency of an open spherical cap, which is a close approximation to a thin-walled, parabolic shell reflector (see the Appendix for details), varies when a ring beam is monolithically attached along the rim. We will show that the stiffness of the fundamental mode of vibration of the spherical cap increases with the cube of the depth of this edge stiffener and, neglecting the mass of the stiffener, the corresponding natural frequency increases with the 1.5 power of the depth of the stiffener.

Consider a thin-walled, isotropic and homogeneous spherical cap, with mid-surface radius, r_s, uniform thickness, t and subtending an angle $2\phi_0$, as shown in Figure 5(a). The Young's

Tan & Pellegrino

modulus, Poisson's ratio and density of the material are denoted respectively by E, ν and ρ.

Figure 5. Cross sections of (a) unstiffened (b) stiffened spherical caps.

A good estimate of the fundamental natural frequency of this shell structure can be obtained[11] by assuming an inextensional mode of vibration of dimensionless amplitude A_i, with i ($=2,3,\ldots$) circumferential waves. Considering a polar coordinate system r, θ, ϕ, the radial components of motion, denoted by the subscript r, have the expression

$$w_r = A_i r_s (i + \cos\phi) \tan^i \frac{\phi}{2} \sin i\theta \tag{10}$$

The corresponding hoop and meridional components are obtained by imposing the condition that no extension takes place.

Rayleigh[11] derived the following expressions for the strain energy, U, and kinetic energy, V, associated with harmonic vibration at angular frequency ω_i

$$U(i, \phi_0) = 2\pi(i^3 - i)^2(1 - \nu)Dg_1(i, \phi_0)A_i^2 \sin^2 \omega_i t \tag{11}$$

$$V(i, \phi_0) = \frac{\pi}{2}\rho t r_s^4 g_2(i, \phi_0)\omega_i^2 A_i^2 \cos^2 \omega_i t \tag{12}$$

where for $\phi = \phi_0$

$$g_1(i, \phi) = \frac{1}{8}\left[\frac{\left(\tan\frac{\phi}{2}\right)^{2i-2}}{i-1} + \frac{2\left(\tan\frac{\phi}{2}\right)^{2i}}{i} + \frac{\left(\tan\frac{\phi}{2}\right)^{2i+2}}{i+1}\right] \tag{13}$$

$$g_2(i, \phi) = \int_0^\phi \left(\tan\frac{\phi}{2}\right)^{2i}\left[(i + \cos\phi)^2 + 2(\sin\phi)^2\right]\sin\phi \, d\phi \tag{14}$$

The form of the equations presented above is largely due to Blevins.[12] Note that D is the flexural stiffness of the shell, i.e.

$$D = \frac{Et^3}{12(1 - \nu^2)} \tag{15}$$

The corresponding natural frequencies of vibration, obtained by equating the maximum

Tan & Pellegrino

strain energy (setting $\sin \omega_i t = 1$) to the maximum kinetic energy (setting $\cos \omega_i t = 1$) in each mode are then

$$f_i = \frac{\omega_i}{2\pi} = \frac{i^3 - i}{2\pi} \sqrt{\frac{E/\rho}{3(1+\nu)}} \sqrt{\frac{g_1}{g_2}} \frac{t}{r_s^2} \quad \text{for } i = 2, 3, 4..... \tag{16}$$

where f_i is the natural frequency of mode $(i-1)$.

For a preliminary estimate of the fundamental natural frequency of a Spring-Back Reflector we assume $r_s = 3100$ mm, $t = 1$ mm, $\phi_0 = 48°$, $E = 40,000$ N/mm^2, $\nu = 0.3$, $\rho = 980$ kg/m^3. Substituting $\phi_0 = 48°$ and $i = 2$ into Equations 13 and 14 gives $g_1 = 0.030$ and $g_2 = 0.033$, and then substituting all of the geometric and material properties of the reflector into Equation 16 gives $f_2 = 0.305$ Hz.

Next, consider adding a light, solid ring beam around the rim of the shell, of cross-sectional dimensions B by T, as shown in Figure 5(b). Note that B is measured on the mid-surface of the spherical shell. It will be assumed that the natural modes of the resulting shell —consisting of a spherical cap clamped to a truncated cone— can be approximated by Equation 10.

To estimate the natural frequencies of this stiffened shell we need to determine the strain energy associated with the chosen vibration mode; the kinetic energy is still given by Equation 12, as the ring beam has been assumed to be light.

Since the assumed vibration modes are unchanged, the strain energy of the stiffened shell is obtained by adding the strain energy of the original shell —given by Equation 11, and which will now be denoted by U_{sphere}— to the strain energy of the ring, U_{ring}. The strain energy of the ring beam can be obtained approximately by considering the difference between a spherical cap of thickness T that subtends an angle ϕ_0 and a spherical cap, also of thickness T, that subtends the smaller angle

$$\phi_1 = \phi_0 - B/r_s \tag{17}$$

Hence we can write

$$U_{\text{ring}}(i) = U(i, \phi_0) - U(i, \phi_1) \tag{18}$$

Equation 18 could be calculated using U given by Equation 11 but, because the width of the edge stiffener is too small for the plate flexural stiffness, D, to be activated, it will be replaced with the bending stiffness per unit width, $ET^3/12$. Hence, we obtain

$$U_{\text{ring}}(i) = \frac{\pi(i^3 - i)^2(1-\nu)ET^3(g_1(i, \phi_0) - g_1(i, \phi_1))A_i^2 \sin^2 \omega_i t}{6} \tag{19}$$

Thus, the frequency of mode $(i-1)$ of the stiffened shell, again obtained by equating maxi-

mum strain and kinetic energies, is

$$f'_i = \frac{i^3 - i}{2\pi}\sqrt{\frac{E}{\rho}}\sqrt{\frac{g_1(\phi_0) + (1-\nu^2)(g_1(\phi_0) - g_1(\phi_1))\left(\frac{T}{t}\right)^3}{3(1+\nu)g_2(\phi_0)}}\frac{t}{r_s^2} \quad \text{for } i = 2, 3, 4..... \qquad (20)$$

We can determine the effectiveness of adding an edge stiffener to a spherical cap by considering the ratio between two corresponding frequencies, and in particular the ratio between the fundamental frequencies. The stiffness ratio is given by the square of the frequency ratios.

Dividing Equation 20 by Equation 16 and simplifying, or alternatively taking directly the square root of the strain energy ratio —since the kinetic energies cancel out— we obtain

$$\frac{f'_i}{f_i} = \sqrt{1 + (1-\nu^2)\frac{g_1(\phi_0) - g_1(\phi_1)}{g_1(\phi_0)}\left(\frac{T}{t}\right)^3} \qquad (21)$$

This equation shows that for any value of i the frequency ratio is proportional to the power 1.5, and the stiffness ratio to the power 3, of the thickness of the stiffener divided by the thickness of the shell. The dependence with the breadth of the stiffener, B is hidden behind the variation of $g_1(\phi_1)$, and is more readily captured by plotting f'_1/f_1 for different widths of the stiffener, see Figure 6.
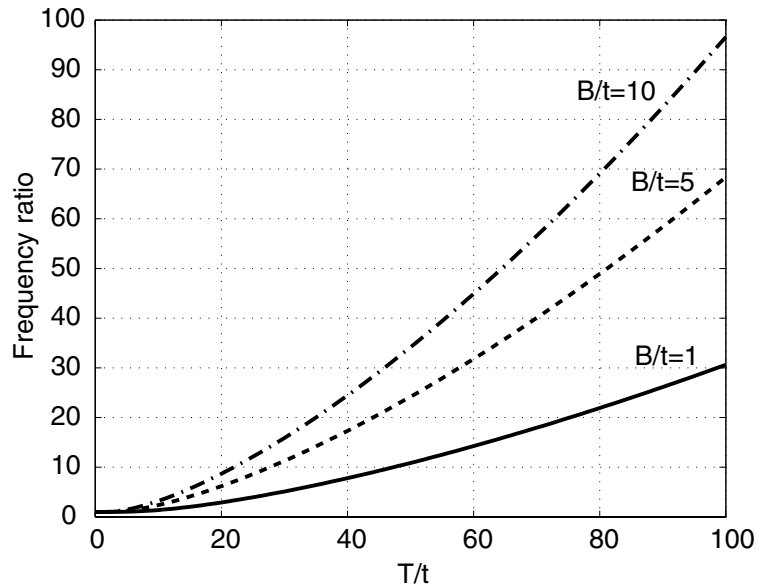
Figure 6. Variation of corresponding natural frequencies with cross-sectional dimensions of stiffener.

From the figure, note that the most efficient way of increasing the fundamental frequency of the reflector is to increase the depth of the stiffener, T. Also note that the frequency increases that can be achieved are potentially very significant. For example the addition of

a 1 mm wide and 40 mm thick stiffener to the edge of the Spring Back Reflector described above (with $B/t = 1$) would increase its fundamental natural frequency from 0.305 Hz to 2.382 Hz, obtained from Equations 16 and 20. More refined estimates of these frequencies, obtained from ABAQUS[13] finite element simulations are 0.301 Hz and 2.840 Hz, respectively.

Note, however, that very deep stiffeners, with $T > \sqrt{r_s t}$, will also have their own vibration modes and, while Equation 20 may still be reasonably accurate in predicting the frequency of the main mode of the dish, the existence of lower frequency modes for the edge stiffener should be expected in such cases.

Also note that —in showing the potential effectiveness of providing an edge stiffener for a thin shell reflector— we have not considered one essential requirement, that the stiffened reflector should not break when it is folded.

V.   Stiffened Reflector Dishes

It has been shown that the addition of a stiffener around the rim of a thin dish greatly increases the stiffness of the structure and hence its fundamental natural frequency. However, a key problem with introducing such a continuous stiffener is that it makes the structure so stiff that it can no longer be folded elastically.

Following the general reasoning presented in Section II, this problem will be addressed by introducing either a small number of radial cuts in the stiffener or circumferential slits between the stiffener and the rim of the dish, which have the purpose of facilitating the folding of the structure without significantly reducing its stiffness in the deployed configuration. A list of the different configurations that have been considered is presented in Table 1, where the diameters d_1 and d_2 are defined in Figure 9(a). A small scale model of the Spring Back Reflector, approximately $1/10^{th}$ scale of a full-size structure, has been used to study the performance of these different stiffened configurations.

A particular type of behaviour that is obtained for some cases is that the cuts/slits allow the stiffener to "snap through" while the reflector is being folded, thus decreasing the force required to fold the reflector and also reducing the peak stresses in the structure. It should be noted that Greschik[4] also introduced cuts in a thin-walled reflector structure to allow the formation of localised folds in the surface, but his analysis of the stresses that occur during folding was purely geometric.

Tan & Pellegrino

	Name	Description
Reference configurations		
	O	Original configuration (unstiffened)
	OS	Continuous stiffener (no cuts, no slits)
Stiffener Configurations with Cuts		
	A0	Cuts along diameter d_1
	A90	Cuts along diameter d_2
	B	Cuts along diameters d_1 and d_2
Stiffener Configurations with Slits		
	C0	Slits at ends of diameter d_1
	C90	Slits at ends of diameter d_2
	D	Slits at ends of diameters d_1 and d_2

Table 1. Configurations of stiffened reflector.

A. Modelling Details

The particular structure that has been analysed has a uniform thickness of $t = 1$ mm and forms an axisymmetric paraboloid of equation

$$z = \frac{x^2 + y^2}{4F} \tag{22}$$

where F is the focal length. The focus to diameter ratio is $\frac{F}{D} = 0.296$, the diameter of the aperture is $D = 452$ mm and hence, the height of the rim above the apex is $h_0 = 95.6$ mm. The material properties were based on a thermoplastic material with the trade name of Vivak,[14] from which several experimental dishes were manufactured.[15] The properties of Vivak are $E = 2$ GPa, $\rho = 1270$ kg/m^3 and $\nu = 0.3$.

The geometry and the finite element mesh were created in the pre-processor PATRAN,[16] see Figure 7. The node and element numbers were then optimized in PATRAN using both the Cuthill and GBBS-Pool-Stk methods.

To keep computational times low, only a quarter of the dish was analysed, using the appropriate boundary conditions. Rigid body motions were constrained by fixing the center of the reflector, Figure 7.

Consistent convergence was achieved with a fine mesh of general purpose, linear 3-noded triangular shell elements (S3R)– average density of 1000 elements per quarter mesh – together with the default ABAQUS iteration control parameters. S3R elements are general purpose shell elements which account for finite membrane strains and will allow for changes in thickness and are therefore, suitable for large-strain analysis. These elements use reduced

Tan & Pellegrino

(lower-order) integration, which significantly reduces run times in three dimensions. According to the ABAQUS manual, these elements provide accurate results, provided that they are not significantly distorted and/or loaded in in-plane bending.[13]
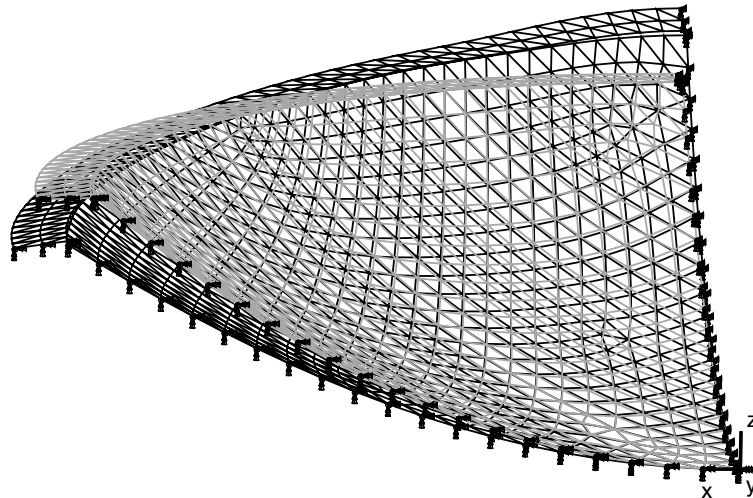
Figure 7. Quarter mesh with boundary conditions. Undeformed mesh (grey) and fundamental bending mode (black).

Depending on the width of the edge stiffener, up to eight uniform rows of S3R elements were used to model this component. These formed a conical surface which was fully-connected to the rim of the parabolic dish, Figure 7. The slits between the dish and the stiffener were modelled by defining two separate sets of geometrically coincident nodes on either side of each slit. The cuts in the stiffener were modelled by simply leaving the respective edges of the stiffener free from any symmetry boundary conditions. See Reference[17] for further details.

All simulations were performed with ABAQUS running on a Pentium III 1 GHz PC; the average run time was less than 20 minutes. A typical analysis consisted of two steps, the first being a linear eigenvalue analysis, to extract the natural frequencies and eigenmodes of the reflector in its deployed configuration, and the second step being a geometrically non-linear simulation of the folding of the reflector.

The first step carries out a *FREQUENCY step, which uses the default 'subspace' eigensolver in ABAQUS, to extract the first 10 eigenmodes. The maximum frequency of interest was set to 20 Hz. The fundamental natural frequency which is used as a measure of the reflector's stiffness in the deployed configuration is obtained from this step.

The second step is a geometrically non-linear static analysis that simulates the folding of the reflector under displacement control. This uses the *STEP, NLGEOM and *STATIC options in ABAQUS. Moving boundary conditions were applied to the rim of the reflector, to impose a total displacement of about $D/2$.

Tan & Pellegrino

The initial slope of the force-displacement relationship, k, which defines the resistance to folding, the maximum stress, σ_{max}, the maximum force that needs to be applied to fold the reflector, F_{max}, and the final value of the force required to hold the reflector in its packaged configuration, F_{final}, were all extracted from this final step.

B.   FE Model Verification

First, the fundamental frequency of the unstiffened reflector obtained from the FE model, 6.0 Hz, was compared to an approximate analytical estimate based on Equation 16.

The spherical equivalent to the structure that is being analysed, see the derivation in the Appendix, has a radius r_s=316 mm and subtends an angle, $\phi_0 = 45.7°$. Substituting these values, and the properties of Vivak into Equation 16, with $g_1 = 0.026$ and $g_2 = 0.025$, gives 6.28 Hz.

The difference between the two values is 4.7% and can be attributed to the fact that the analytical estimate is for a spherical, not a parabolic shell. The FE estimate increases to 6.28 Hz if the geometry is modified to a spherical cap.

Next, it was verified that the quarter-models set up in ABAQUS yield similar results to the corresponding full models of the structure. Figure 8 shows force-displacement curves for configurations A90 (parameters: $w = 22$ mm, $\theta = 50°$ and $t = 1$ mm) and D (parameters: $w = 10$ mm, $\theta = 50°$ $\eta = 12°$, $\gamma = 4°$, $t = 1$ mm). For A90 the discrepancies between the two models are negligible. For configuration D the quarter model reaches a 3% higher peak force and predicts a slightly lower final force. Two different full models have been analysed, one with two planes of mirror symmetry and the other obtained by rotating the quarter mesh about the z-axis; practically no difference was found between these two cases.

Despite the closeness of the results obtained from the quarter and full models, care needs to be taken when performing eigenvalue analyses. It was found that for certain cases a second bending mode, at a frequency very close to that of the first bending mode, was captured by the whole model but not by the quarter model. This mode was observed in a series of experiments on physical models.[15] Hence, whereas in all optimization runs the quarter model was used —to save computing time— as the mode of interest is the lowest bending mode which is easily captured by the quarter model, the full model was used for all experimental verification work. Finally, note that the fundamental frequency of the configuration D quarter model considered above is 19.5 Hz while that of the full model is 19.6 Hz; the difference is only 0.5%.

C.   Stiffener Design Parameters

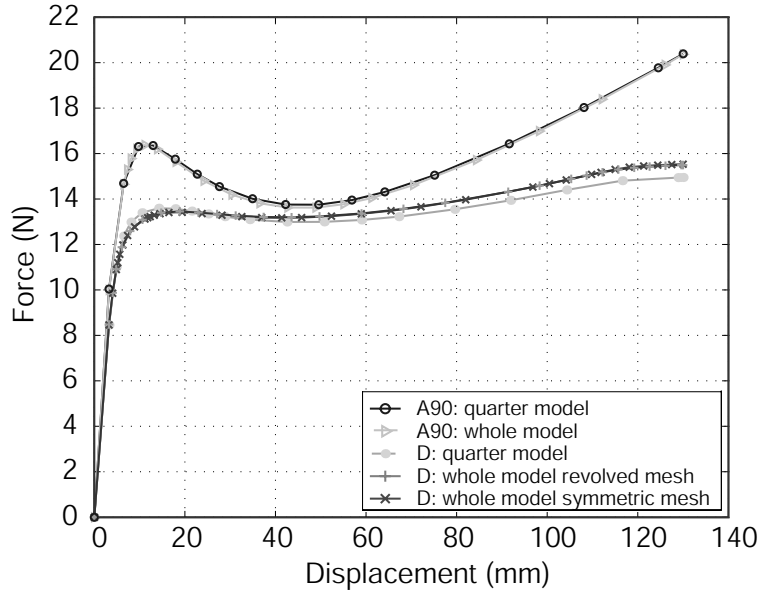The design parameters for the edge stiffener are, see Figure 9:

Tan & Pellegrino

Figure 8. Comparison of force-displacement response from different ABAQUS models.

- The width, w, and thickness of the stiffener, B.

- The apex angle, θ, of the conical surface.

- The number of cuts, the number of slits, and their location.

- The angles subtended by the slits, γ and η.

where it should be noted that, on the basis of preliminary experimentation on simple physical models, the range of options for the number and location of the cuts/slits is restricted to those listed in Table 1. Also, it was decided that the thickness of the stiffener would be set equal to that of the main shell, i.e. $B = t$, for simplicity.

To obtain an indication of the effectiveness of each design parameter in increasing the fundamental natural frequency of the chosen small scale reflector, while also evaluating the effect it has on increasing the maximum stress in the folded reflector, a series of preliminary studies were carried out on configurations A90, B, and D only. In each study, only one design parameter was modified, starting from a common initial design.

First, the effect of increasing the stiffener width, w, was considered —assuming the stiffener to be a flat horizontal plate (i.e. a cone with $\theta = 90°$) with either two or four cuts. Figure 10(a) shows that the frequency increases rapidly for $w < 20$ mm for configuration A90 and $w < 10$ mm for configuration B, but both decrease for $w > 20$ mm.

This is because the frequency is dependent on the ratio between modal mass and stiffness and, as w increases, so does the mass. Beyond a certain limit, the mass penalty associated with increasing w outweighs the increase of stiffness provided. This result is somewhat

Tan & Pellegrino

(a) Views along z-axis (deployed and folded)

(b) Cross section
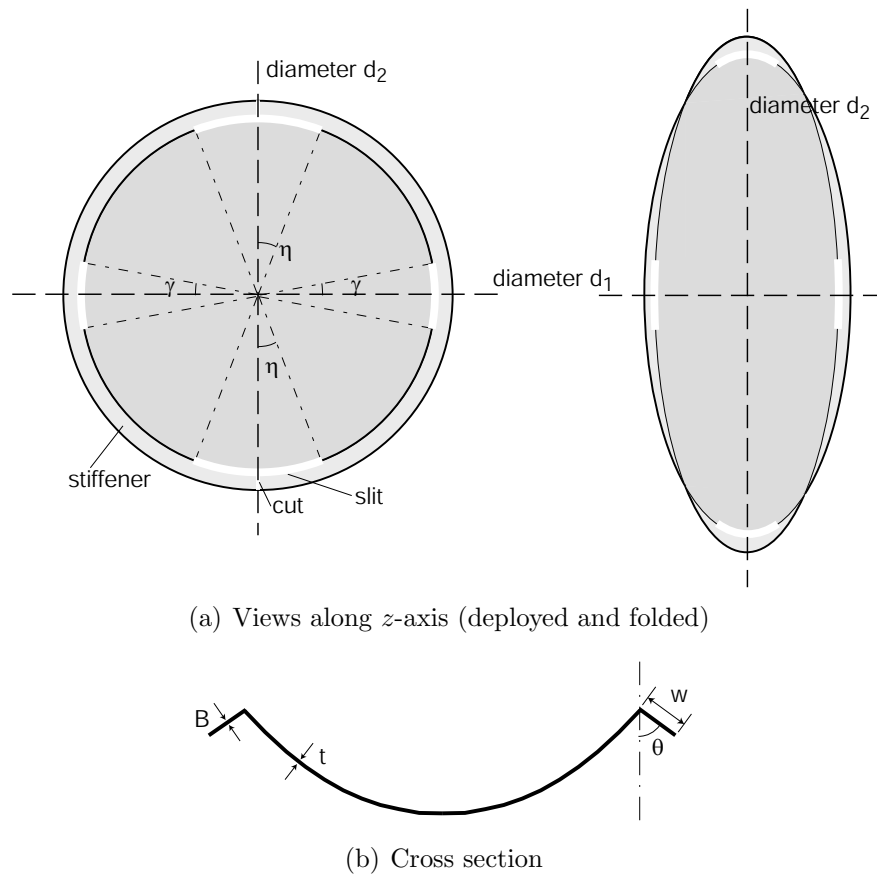
Figure 9. Design parameters of stiffener.

different from the power law relationship in Equation 21, which assumed the added mass to be negligible, the stiffener to be perpendicular to the shell surface and no cuts.

The effect of w on the maximum stress in the packaged reflector is plotted in Figure 10(b). Increasing the width of the stiffener increases the stress, initially at a faster rate.

Second, the effect of varying the angle of the stiffener was considered, for the cases of either two or four cuts. The results are shown in Figure 11. Both the frequency and stress variations are roughly bilinear; the maximum frequency occurs around $\theta = 80°$, which is close to the stiffener being a flat plate. This increase of stiffness is coupled with the penalty of increased maximum stress in the packaged configuration, Figure 11(b).

The above results show that, although effective in increasing the deployed frequency, the introduction of radial cuts in the the stiffener leads to high peak stresses. These high stresses arise from having localized the bending of the main dish near the apex of the cuts, and hence the maximum stress is relatively insensitive to the addition of radial cuts along diameter d_1.

This sharp localization in the bending of the surface is avoided in configuration D. This is because the slits allow a larger area of the dish to bend, rather than concentrating the curvature change along a narrow region of the dish. Two pairs of diametrically opposite
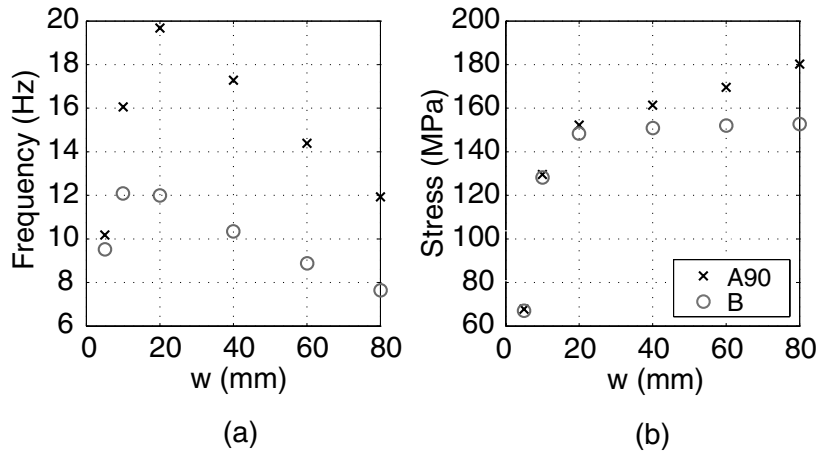
Tan & Pellegrino

Figure 10. Variation of fundamental deployed frequency and maximum packaged stress with stiffener width, for $\theta = 50°$.
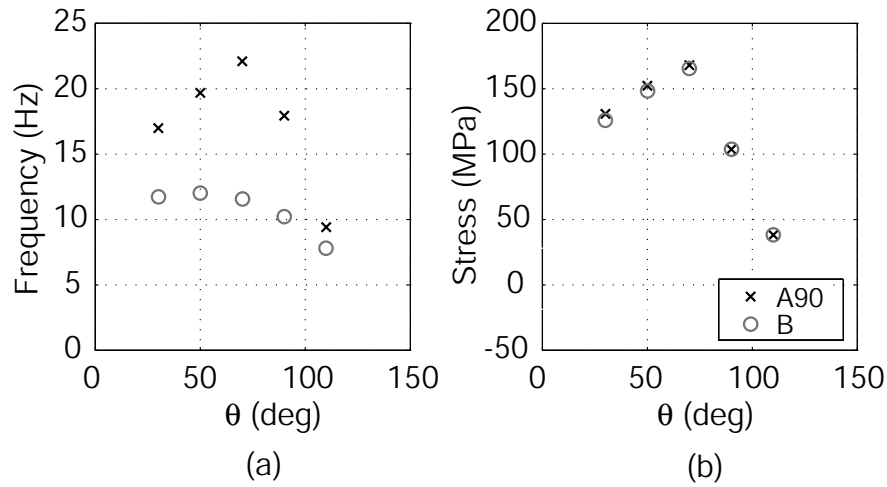

Figure 11. Variation of fundamental deployed frequency and maximum packaged stress with stiffener angle, for $w = 20$ **mm**.

slits were considered in the present study; the resulting load-displacement plots are shown in Figure 12.

The pair of slits at the end of diameter d_2 serve the purpose of allowing larger portions of the dish to deform, and so reduce the peak strains in the folded dish. They also control the final force required to keep the reflector packaged; increasing the slit angle η reduces these forces. On the other hand, the pair of slits at the end of diameter d_1 allow the stiffener to buckle during packaging, and hence affect the initial stiffness of the reflector.
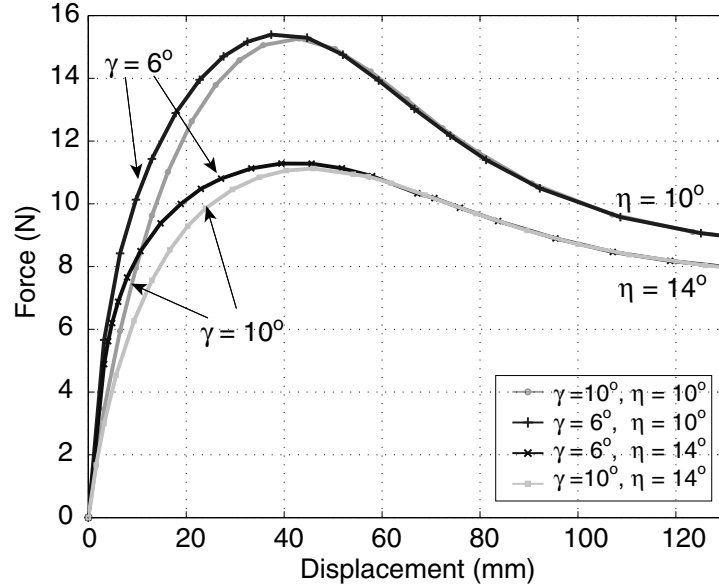
Figure 12. Variation of folding force-displacement relationship with stiffener slit angles, for $w = 20$ mm and $\theta = 50°$.

D.   Packaging

An analysis of the packaging force-displacement relationship of the reflector provides significant insight into the behaviour of the structure and is also useful in making comparisons between different designs of the edge stiffener. The reflector structure is folded about diameter d_2 which is equivalent to applying two diametrically opposing forces, F along diameter d_1 – causing it to fold in a way similar to Figure 1

This relationship has been computed for the eight different design configurations listed in Table 1, see Figure 13. Note that the displacement plotted in Figure 13 is that of *one* loaded point; the point diametrically opposite moves by an equal but opposite amount. In all cases, the stiffener width is $w = 20$ mm, its angle $\theta = 50°$, and the slit angles where applicable are equal, $\eta = \gamma = 10°$.

The unstiffened reflector, O, and the reflector with a continuous stiffener but neither slits nor cuts, OS, i.e. the configurations with minimum and maximum initial stiffness, were analysed to obtain two reference curves. In all cases it was assumed that the behaviour of the material is linear-elastic, regardless of strain magnitudes.

Table 2 compares key characteristics of these different configurations. Columns 2 to 4 list the ratios between the initial (i.e. tangent) stiffness in the deployed configuration, k, the fundamental natural frequency of vibration, f, the final packaging force, F_{final}, and the maximum force reached during packaging, F_{max}, —for each design configuration— with respect to the unstiffened reflector, whose values are denoted by the subscript 0. Column 5 lists the ratios between the final and maximum force. Column 6 lists the maximum stresses,
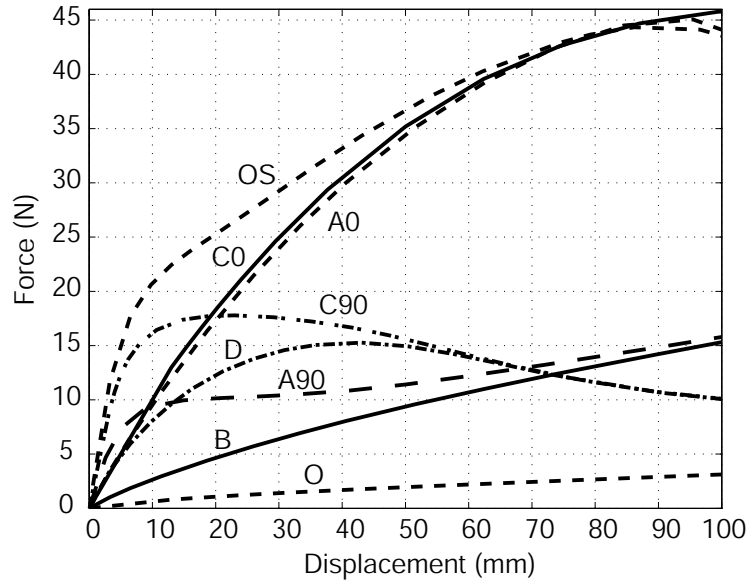
Figure 13. Force-displacement plots for eight different designs.

σ_{max}, in the packaged reflector assuming the structure to be made of Vivak and yet to remain linear-elastic regardless of the large stress magnitude.

Configuration	k/k_0	f/f_0	F_{final}/F_{final_0}	F_{final}/F_{max}	$\sigma_{max}(MPa)$
O	1.0	1.0	1.0	1.0	10
OS	53.2	5.0	13.9	1.0	181
A0	17.4	3.3	14.1	1.0	179
A90	27.2	3.3	5.1	1.0	152
B	5.0	1.6	6.0	1.0	151
C0	16.5	4.2	14.7	1.0	100
C90	46.1	4.2	3.2	0.6	85
D	16.7	3.5	3.2	0.7	84

Table 2. Key characteristics of different structural configurations.

It is useful to discuss the response curves by grouping them into sets that share common features, as follows.

1. Very low initial stiffness and very low packaging force – Configuration O. The unstiffened configuration has an initial stiffness of 0.06 N/mm and a final packaged force of 3.1 N.

2. Low initial stiffness and high packaging force – Configuration B. The reason for the high packaging force is that the reflector folds into two almost rigid half-shells connected by an elastic hinge aligned with the two cuts. The transverse curvature in this hinge region

increases with the amount of folding and its longitudinal curvature is approximately zero. Hence, after some initial non-linearity the force displacement relationship is almost linear. However, note that Configuration B has the lowest initial stiffness among all stiffened configurations, despite a 5 fold increase on Configuration O.

3. High initial stiffness and low packaging force – Configuration D. This configuration exhibits a high initial stiffness (16.7 times higher than Configuration O) but then gradually softens and so the final packaging force is only about double that of the unstiffened reflector. Note that Configuration D also has the lowest packaged stresses among all stiffened configurations.

4. High initial stiffness and high packaging force – Configuration A90. Its initial stiffness (1.6 N/mm) is over five times that of Configuration B, due to the smaller number of cuts, however its large displacement characteristics tend towards that of Configuration B.

5. High initial stiffness and very high packaging force – Configurations A0 and C0. These two configurations show very similar folding behaviours, despite one having cuts and the other slits. The reason is that the folding deformation is in both cases concentrated in regions where there are no cuts or slits. Hence in the large displacement regime the behaviour of both configurations approaches that of Configuration OS. Comparing Configurations A0 and C0 with Configuration OS, the initial stiffness is much lower, and hence it can be concluded that the slits or cuts at the ends of diameter d_1 play a key role in determining the initial stiffness of the reflector.

   However, if we compare k and σ_{max} there are some important differences between Configurations A0 and C0. C0 has a higher deployed stiffness, due to the fact that the edge stiffener is continuous, whereas the discontinuous stiffener in Configuration A0 is less effective (due to the introduction of two cuts). Furthermore, the cuts in Configuration A0 lead to higher stress concentrations at the apexes of the cuts.

6. Very high initial stiffness and low packaging force – Configuration C90. As for Configuration D, there is a gradual softening response, however this time the initial stiffness is higher, but the large displacement behaviour is identical to Configuration D.

   Configuration C90 is particularly interesting; its initial stiffness is 46 times higher but the force required to hold it folded is only 2.3 times higher than for Configuration O. Indeed, this configuration has both the highest initial stiffness and deployed frequency of all non-reference configurations, together with the second-lowest packaged stress and final packaged force.

Tan & Pellegrino

7. Very high initial stiffness and high packaging force — Configuration OS. This is obviously the stiffest possible arrangement which suffers from the highest maximum stresses of all configurations and is hence not a viable option.

A characteristic common to the two most interesting configurations emerging from this study, C90 and D, is that they are the only two that show snapping behaviour after an initially linear response. This is is also evident from Column 5 in Table 2 as ratios of $F_{final}/F_{max} < 1$ indicate 'snapping' – the lower the value the more pronounced the snapping behaviour. This type of behaviour is very desirable as the structure *locks into the fully-deployed configuration* and yet it *folds rather easily, after some initial resistance.* The presence of long slits at the end of diameter d_2 has the effect of spreading the deformation of the dish, when it is folded, over a wider region than when radial cuts are used.

The decrease in initial stiffness from Configuration C90 to Configuration D is due to the introduction of two rather long slits at the end of diameter d_1. Hence, these slits should be as short as possible, and certainly not of equal length to those at the end of diameter d_2.

VI.   Optimal Configuration

Taking Configuration D as a starting point, an optimization study was performed to determine the best values of the parameters θ, w, γ, η (defined in Figure 9) that control the design of the collapsible stiffener. The objective was to maximize the deployed stiffness, represented by the fundamental deployed frequency, f, subject to the maximum stress, σ_{max}, in the packaged reflector being smaller than a set limit.

It needs to be noted that in considering the maximum stress in the packaged reflector, the stresses around the tips of the slits were neglected. For the optimization study, the slits were modelled as long voids of finite width –rather than unconnected portions between the dish and stiffener– hence the very high tip stresses in the first finite width element at each slit end were neglected. These are regions of very high stress concentrations, but it has been shown[18] that detailed redesign of these regions, by rounding the corners and/or grading the stiffness of the material, can reduce these stresses to values close to those that occur elsewhere in the reflector. This redesign is best carried out as a separate step, after determining the overall stress distribution of stress in the folded reflector.

An automatic mesh generation procedure was created, and the Hooke & Jeeves direct search method was used to find a series of optimal configurations. Details of this study will be published in a separate paper.[17]

An optimal Configuration D, obtained for $\sigma_{max} = 26$ MPa, is presented in Table 3. The corresponding values of the design parameters are;

- apex angle of stiffener, $\theta = 88.1°$

Tan & Pellegrino

- width of stiffener, $w = 20$ mm

- angle of slit at end of diameter d_1, $\gamma = 6.1°$

- angle of slit at end of diameter d_2, $\eta = 17.4°$

Figure 14 compares the load-displacement relationship of this optimised structure (Optimal D) with the original, unstiffened structure (O) and a stiffened structure with only two slits (C90), which however, has a maximum stress well in excess of the specified limit. This C90 configuration is identical to Optimal D except for the fact that the pair of slits at the ends of diameter d_1 have been removed, i.e. $\eta = 17.4°$ and $\gamma = 0°$.

Configuration	k (N/mm)	f (Hz)	F_{final} (N)	σ_{max} (MPa)	Mass (kg)
O	0.06	6.00	3.10	9.98	0.236
Optimal D	1.88	24.13	4.11	25.91	0.274
C90	2.72	24.76	4.18	39.18	0.274

Table 3. Comparison of optimized Configuration D.
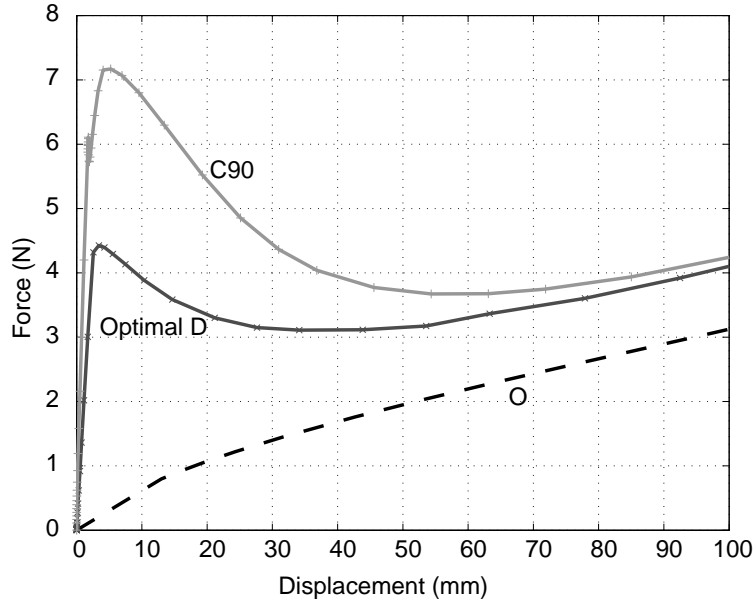
Figure 14. Comparison of force-displacement relationship of optimized Configuration D with original unstiffened configuration (O) and 2 slit configuration (C90).

More detailed information on the stress distribution in the folded structure is presented in Figure 15. It can be observed that the highest stresses occur in the unsupported regions of the stiffener; the first region of high stress being the stiffener region adjacent to the shorter slit and the second region being the area surrounding the tip of the longer slit.

Tan & Pellegrino
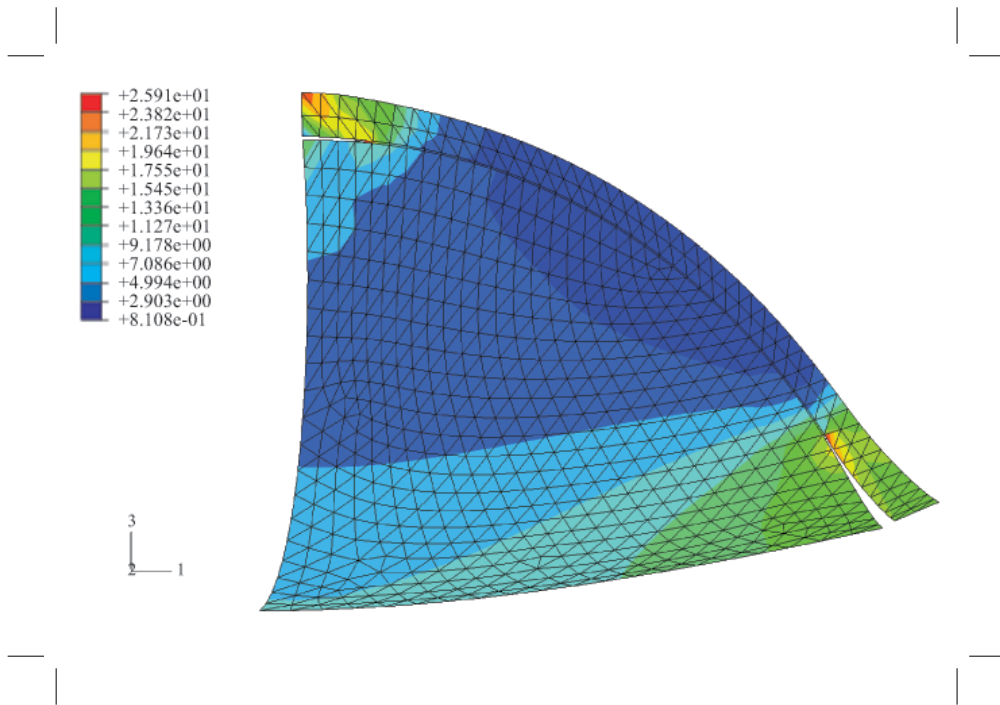
Figure 15. Von Mises stress distribution for optimized Configuration D, in MPa.

VII.   Discussion and Conclusion

The simple analytical estimates presented in Section IV have allowed us to quantify the increases in a thin-shell reflector's deployed stiffness, and fundamental natural frequency of vibration, that are achieved through the addition of a thin stiffener around the rim of the reflector structure. It has been shown that 10-fold increases in frequency can be achieved quite easily. Hence, increasing the deployed stiffness of a thin-shell reflector structure is not difficult, but the key problem is ensuring that the stiffened structure can still be folded elastically.

Two different ways of achieving stiffer reflectors that can still be folded have been explored, through the introduction of (i) cuts or (ii) slits in the stiffener. The first approach, with cuts in the stiffener, tends to concentrate the deformation of the folded reflector in a narrow strip. This results in maximum stresses that are at least 15 times larger than the maximum stress in the unstiffened dish. The second approach, with circumferential slits, spreads the deformation over a wide region, whose width is largely controlled by the length of the slits at the end of diameter d_2. Hence, it has been concluded in the paper that the introduction of slits between the dish and the stiffener is the most effective way forward.

Varying the length of the two pairs of slits is a way of controlling the stiffness of the deployed reflector, the maximum disturbance force that it will withstand without starting to fold, and the maximum stress in the folded reflector. Very broadly speaking, for a stiffener

Tan & Pellegrino

of given width and thickness, shortening the slits at the end of diameter d_1 increases the stiffness, whereas shortening the slits at the end of diameter d_2 has the effect of increasing the maximum stress in the folded reflector. The magnitude of the maximum force before the reflector snaps is controlled by both sets of slits, and increases when they are shorter.

The specific case of a Vivak dish with aperture diameter of 452 mm, thickness of 1 mm, and focal length to diameter ratio of 0.296 has been considered. It has been shown that its stiffness in the deployed configuration increases by a factor of 53.2 when a 20 mm wide and 1 mm thick edge stiffener is continuously connected to the edge of the reflector. However, the penalty associated with this design modification is an 18-fold increase in the maximum stress in the folded reflector, which would be well in excess of the yield stress.

Hence, having assumed that Vivak would remain close to linear-elastic for stresses up to 26 MPa, this value was set as a limit when searching for an optimized set of design parameters. One of the optimal configurations that was arrived at has a 20 mm wide by 1 mm thick stiffener that is nearly planar (the optimal value of the cone angle was 88.8°, i.e. almost 90°); the slits at the end of diameter d_1 subtend a total angle of almost 35° whereas the second set of slits are about one-third this length. This configuration is 31 times stiffer but is only 16% heavier than the unstiffened dish, and has a maximum stress within the prescribed limit.

The force-displacement relationship for this optimized configuration is shown in Figure 14. The significant increase in initial stiffness with respect to the unstiffened dish, and the snapping behaviour of the stiffener, whereby the forces needed to package the dish suddenly decrease, are evident in the figure. Non-optimized configurations tend not to show such a pronounced snapping behaviour.

It is also insightful to make a further comparison with the corresponding non-reference configuration (C90) which was shown in Section V to have the highest deployed stiffness and frequency. Figure 14 shows a 42% increase in maximum 'snapping' force, F_{max} but an almost identical final packaged force, F_{final}. The ratios of F_{final}/F_{max} are 0.84 and 0.60 for configurations Optimal D and C90 respectively. This 2 slit configuration has a 16% higher initial stiffness but a 50% increase in packaged stress – well in excess of the specified limit. The only difference between these two configurations is the absence of slits at the end of diameter d_1, hence C90 is the limiting case of D and this demonstrates the tunability of configuration D.

In conclusion, the viability of stiffening a thin shell deployable reflector by putting a collapsible stiffener, which still allows for elastic folding and completely passive deployment, around its rim has been demonstrated. Key to this scheme are two pairs of circumferential slits which allow localised elastic buckling of the stiffener, hence significantly reducing the stiffness of the reflector when it is being packaged. The performance of the stiffener can

be enhanced significantly by optimizing its design parameters. A small number (four) of adjustable parameters have been considered so far and a 70% reduction in the maximum stress in the folded reflector has been achieved, without any significant reduction in the stiffness of the reflector.

Acknowledgments

A. Appendix: Derivation of Spherical Equivalent to a Parabolic Cap

A spherical cap that approximates to a paraboloidal cap can be determined based on the assumption that both caps have the same aperture diameter, D and rim height, h_0, Figure 16. The spherical cap is fully described by the radius, r_s, and the angle subtended, ϕ. From triangle I in Figure 16,
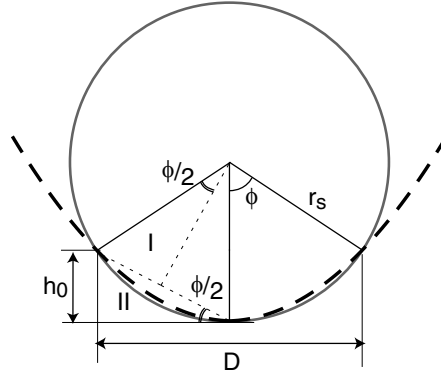

Figure 16. Approximation of paraboloid with a spherical cap.

$$\sin \frac{\phi}{2} = \frac{\sqrt{\left(\frac{D}{2}\right)^2 + h_0^2}}{2r_s} \tag{23}$$

While from triangle II,

$$\sin \frac{\phi}{2} = \frac{h_0}{\sqrt{\left(\frac{D}{2}\right)^2 + h_0^2}} \tag{24}$$

Combining Equations 23 and 24, and solving for r_s,

$$r_s = \frac{1}{2}\left(\frac{D^2}{4h_0} + h_0\right)$$

For a parabola with focal length F, the height of the rim, h_0, is

$$h_0 = \frac{D^2}{16F} \tag{25}$$

Substituting into Equation 25 results in

$$r_s = 2F + \frac{D^2}{32F} \tag{26}$$

Next the subtended angle, ϕ, of the spherical cap needs to be determined. From Figure 16

$$\sin\phi = \frac{D/2}{r_s} \tag{27}$$

hence the subtended angle of the spherical cap is

$$\phi = \sin^{-1}\left(\frac{D}{2r_s}\right) \tag{28}$$

$$= \sin^{-1}\left(\frac{D}{2F + \frac{D^2}{32F}}\right) \tag{29}$$

References

[1]Rimrott, F. P. J., "Storable Tubular Extendible Member," *Machine Design*, Vol. 37, 1965, pp. 156–165.

[2]Aguirre, M., Bureo, R., Fuentes, M., and Rivacoba, J., "The Collapsible Tube Mast (CTM)," *Second European Space Mechanisms and Tribology Symposium*, Meersburg, Germany, 9-11 October 1985, pp. 75–81.

[3]Givois, D., Sicre, J., and Mazoyer, T., "A Low Cost Hinge for Appendices Deployment: Design, Test and Applications," *9th European Space Mechanisms and Tribology Symposium*, Liege, Belgium, 19-21 September 2001.

[4]Greschik, G., "On the Practicality of a Family of Pop-up Reflectors," *9th Annual AIAA/Utah State University Conference on Small Satellites*, 18-21 September 1995.

[5]Romeo, R. C., Meinel, A. B., Meinel, M. P., and Chen, P. C., "Ultra-lightweight and Hyperthin Rollable Primary Mirror for Space Telescopes," *UV, Optical and IR Space Telescopes and Instruments,Proceedings of SPIE*, edited by J. Breckinridge, Vol. 4013, 2000, pp. 634–639.

[6]Tibbalds, B., Guest, S. D., and Pellegrino, S., "Inextensional Packaging of Thin Shell Slit Reflectors," *Technische Mechanik*, Vol. 24, No. 3-4, 2004, pp. 211–220.

[7]Seizt, P., "Spar Resolving Spat Over Antenna Work," Space News, Aug 29 - Sept 4 1994.

[8]Anonymous, "Hughes Graphite Antennas Installed on MSAT-2 Craft," Space News, November 1994.

[9]Robinson, S. A., "Simplified Spacecraft Antenna Reflector for Stowage in Confined Envelopes," Publication number: 0534110A1, 31 March 1993, European Patent Application filed by Hughes Aircraft Company.

[10]Rogers, C. A., Stutzman, W. L., Cambbell, T. G., and Hedgepeth, J. M., "Technology Assessment and Development of Large Deployable Antennas," *ASCE J. Aerospace Engineering*, Vol. 6, No. 1, 1993, pp. 34–54.

[11]Rayleigh, J. W. S., *The Theory of Sound*, Vol. 1, Dover Publications New York, 1945.

[12]Blevins, R. D., *Formulas for Natural Frequency and Mode Shapes*, chap. 12, Krieger Publishing Company, pp. 330–334.

[13]Hibbitt, Karlsson, and Sorenson, *ABAQUS Standard Users Manual Version 6.1*, Hibbitt, Karlsson and Sorenson Inc., 1080 Main Street Pawtucket, Rhode Island 02860-4847 , USA, 1998.

[14]"Vivak Product Technical Data Sheet," http://www.sheffieldplastics.com, [cited 3 February 2005].

[15]Tan, L. T. and Pellegrino, S., "Stiffening Method for Thin Shell Deployable Reflectors: Part II – Experiments, Approach," To be submitted to AIAA Journal.

[16]MacNeal-Schwendler Corporation, *MSC/PATRAN Version 8.5*, MSC Software, Los Angeles, California, USA, 1999.

[17]Tan, L. T. and Pellegrino, S., "Stiffness Optimization for Reflector Antennas," To be submitted to Computers & Structures.

[18]Tan, L. T., *Thin-Walled Elastically Foldable Reflector Structures*, Ph.D. thesis, Department of Engineering, University of Cambridge, Cambridge, CB2 1PZ, UK, December 2002.